Design of midinfrared photodetectors enhanced by surface plasmons on grating structures

Zongfu Yu,[a] Georgios Veronis, and Shanhui Fan
Ginzton Laboratory, Stanford University, Stanford, California 94305

Mark L. Brongersma
Geballe Laboratory of Advanced Materials, Stanford University, Stanford, California 94305

(Received 6 July 2006; accepted 23 August 2006; published online 11 October 2006)

The authors propose to exploit the unique properties of surface plasmons to enhance the signal-to-noise ratio of midinfrared photodetectors. The proposed photodetector consists of a slit in a metallic slab filled with absorptive semiconductor material. Light absorption in the slit is enhanced due to Fabry-Perot resonances. Further absorption enhancement is achieved by surrounding the slit with a series of periodic grooves that enable the excitation of surface plasmons that carry electromagnetic energy towards the slit. Using this scheme, they design and optimize a photodetector operating at $\lambda_0=9.8$ μm with a roughly 250 times enhancement in the absorption per unit of volume of semiconductor material compared to conventional photodetectors operating at the same wavelength. © *2006 American Institute of Physics*. [DOI: 10.1063/1.2360896]

Midinfrared photodetectors and imaging systems operating in the vicinity of 10 μm wavelength are important in applications ranging from night vision to astronomy research.[1] To suppress noise caused by thermal fluctuation, usually these detection systems have to be cooled,[1–3] which greatly increases the cost and limits the portability. To improve signal/noise ratio, it is desirable to reduce the active detector volume from which the noise arises without affecting the absorbed light power.

In this letter, we computationally explore the use of surface plasmons in these systems to improve the signal/noise ratio. The proposed structure, shown in Fig. 1(a), consists of a metallic slit, surrounded by a linear grating structure. The entire structure is placed on top of an insulating oxide. The slit is filled with absorptive semiconductor material, and has a width that is far smaller than the operating wavelength. The metal regions serve both as electrical contacts and as a concentrator that funnels light into the deep-subwavelength slit.[4–6]

To maximize the concentration effects, we combine two distinct mechanisms that relate to the presence of the slit and the grating structure.[7] A metal slit supports a propagating TE mode, even when the width of the slit is at deep-subwavelength scales. Moreover, due to the strong impedance mismatch between the modes in the slit and free-space propagating waves, strong reflection can occur at the entrances to the slit. Consequently, with an appropriate choice of the length, the slit forms a Fabry-Perot resonator, and light absorption in the slit is resonantly enhanced. The grating, on the other hand, enhances the light absorption in the slit by converting incident electromagnetic (EM) waves into surface plasmons on the metal surface that can be funneled into the slit.[8] The area from which EM energy is collected can be substantially larger than the slit width and gives rise to significant enhancements in the absorbed energy. With a careful choice of the geometric parameters of the structure, these two mechanisms can be made to occur at the same wavelength, resulting in an optimized efficiency of the devices.

To simulate the response of this structure for a normally incident EM plane wave, we use a two-dimensional finite-difference frequency-domain method,[9,10] which directly uses experimental data for the frequency-dependent dielectric constant of metals such as gold,[11] including both the real and imaginary parts, with no further approximation. For the detective materials in the slit, we have chosen to use HgCdTe (MCT) with a frequency independent dielectric permittivity of $\varepsilon=12.5+i1.75$.[2,11] The substrate is a low-index oxide

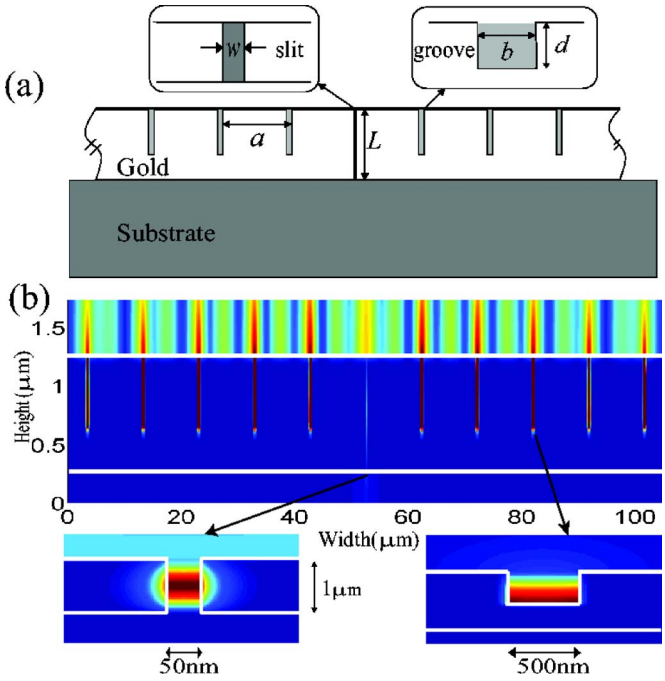

FIG. 1. (Color online) (a) Device geometry. It consists of a gold slab on a low-index oxide ($\varepsilon=2.25$) substrate. The central slit through the slab is filled with mercury cadmium telluride (MCT), the active detector material. A periodic set of grooves is patterned on both sides. The insets show the magnified views of the slit and one of the grooves. The slab is infinitely long but the number of the grooves N_g is finite. (b) Magnetic field pattern for a device with $a=9.8$ μm, $L=1.0$ μm, $w=50$ nm, $b=0.5$ μm, $d=0.6$ μm, and $N_g=15$, operating at $\lambda_0=9.8$ μm. The insets show the magnified views of the field in the central slit and in one of the grooves.

[a]Electronic mail: zfyu@stanford.edu

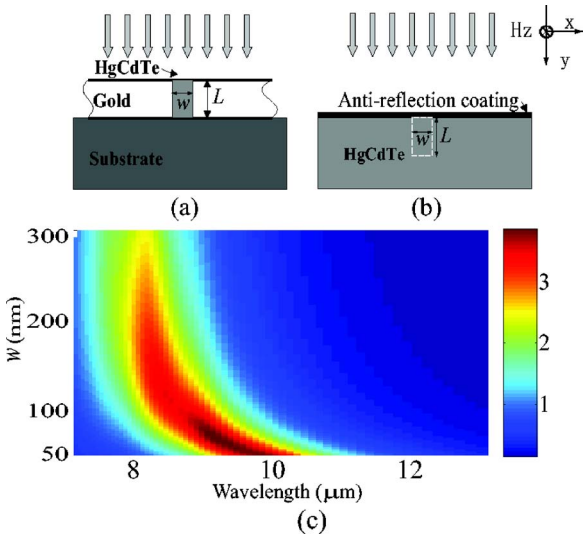

FIG. 2. (Color online) (a) Geometry of a device consisting of a single slit. (b) Geometry of a bulk MCT photodetector with an antireflection coating. (c) Absorption cross section in units of w for the structure in Fig. 2(a) with $L=1$ μm as a function of the slit width w and wavelength.

($\varepsilon=2.25$). We also apply the total-field-scattered-field formulation[12] to simulate the response of the structure to a plane wave input.

An important aspect regarding the computational modeling of plasmonic devices is the presence of multiple relevant physical length scales that are drastically different. The enhancement of the field inside the slit requires a deep subwavelength slit width w of about 50 nm. Thus the minimum spatial resolution needs to be a few nanometers. On the other hand, the pitch of the grating a should be equal to the wavelength of the surface plasmon, i.e., $a\sim10$ μm, in order to efficiently convert normally incident EM waves to surface plasmon waves. In our simulations, a typical calculation consists of a computational cell size of 200×70 μm and the minimum grid size of 2.5 nm. The use of a uniform grid would thus require $\sim10^9$ grid points. On the other hand, recognizing that the finest grid only needs to be employed in the vicinity of the slit and the grooves, we use a nonuniform orthogonal grid[12] to greatly reduce computational costs. For the same structure, we use a 2.5 nm/grid point resolution for the slit, 20 nm/grid point for the grooves, and 250 nm/grid point for intergrooves spacing. Smooth transition regions are used between high and low resolution regions. The number of grid points in this construction is $\sim10^5$, making the simulation far more computationally tractable. A comparison between the uniform and nonuniform grids with a test structure shows that the calculated flux through the slit differs by less than 0.1%.

For comparison of different configurations, we define the *absorption cross section* of the detector as the total light power absorbed by detector material (MCT) in the slit, normalized by the incident plane wave flux [Fig. 2(a)]. In two dimensions, the cross section is in the unit of length. We also calculate such an absorption cross section for the same volume of detector material in a uniform thick slab with an antireflection coating, which is a typical configuration for conventional detectors [Fig. 2(b)]. The ratio between these two absorption cross sections defines the *enhancement factor*, since it measures the enhancement of the light absorption per unit of volume of detector materials. This factor is proportional to the improvement of the signal/noise ratio, because the thermal noise is primarily determined by the volume of the active detector material.

As the first step of the design process, we optimize a single slit in an otherwise uniform gold slab[13] [Fig. 2(a)].We chose the length of the slit $L=1$ μm so that the lowest-order Fabry-Pérot resonance of the slit occurs a little below $\lambda_0\sim10$ μm. The resonance wavelength is then fine tuned by adjusting the width of the slit w. Figure 2(c) shows the dependence of the absorption cross section on the slit width w and wavelength for $L=1$ μm. As the width w decreases, the peak of the absorption cross section, which corresponds to the Fabry-Pérot resonance, shifts towards longer wavelengths due to the increasing effective index of the propagating mode in the slit. As the slit width w decreases, more modal fields are distributed in the metal resulting in a higher effective index for the mode.[14] Also, as the width w decreases, the ratio of the absorption cross section to the slit width w increases due to the enhanced field intensity with narrower width.[15] At the resonant peak, we find that $\sim$70% of the power entering into the slit is absorbed by the MCT material because the slit mode has a higher group index compared with MCT material alone. Moreover, a deep subwavelength slit collects light from a larger area than its geometrical aperture size. As an example, for a slit with a width of 50 nm, the transmitted power into the slit is equal to the plane wave power incident on an approximately five times wider aperture. Since $\sim$70% of transmitted power is absorbed by MCT, the overall absorption cross section is $\sim3.5w$ [Fig. 2(c)]. In comparison, less than 30% of the incident power is absorbed over the same length L of bulk MCT material corresponding to an absorption cross section of $\sim0.3w$. Thus, the use of a single metal slit results in an enhancement factor of $\sim$10.

To further enhance the performance of the device, we use a grating consisting of a set of periodic grooves. In this way, light is collected from a much larger area than the geometrical slit area and is subsequently "funneled" into the detector material. The scattering strength of a groove is approximately proportional to the field strength inside the groove from an incident plane wave. Therefore, the groove width b and depth d [Fig. 1(a)] are chosen using a procedure similar to slit optimization, such that the first groove resonance occurs at the operating wavelength. Since the slit is filled with MCT ($\varepsilon_{\text{real}}=12.5$), to ensure that $d<L$ high-index material ($\varepsilon=12.5$) inside the grooves is required. Due to the boundary condition at the bottom of the groove, $d\approx L/2$. Starting from this initial guess of the groove depth, the geometrical parameters of the groove are then optimized by maximizing the field intensity inside the groove at the operating wavelength. For a device operating at a wavelength of $\lambda_0\sim9.8$ μm, this procedure gives $b=0.5$ μm and $d=0.6$ μm.

For a normally incident plane wave, the maximum coupling to the surface plasmon mode occurs when the grating period a [Fig. 1(a)] is equal to the surface plasmon wavelength, as dictated by the Bragg condition. Thus, in midinfrared the optimized grating period should be in the vicinity of the operating wavelength.

In order to maximize the enhancement, one needs to align the resonance wavelengths of the groove, the slit, and the grating.[7] In Fig. 3, we compare two structures with the same slit width $w=50$ nm, corresponding to a slit resonance

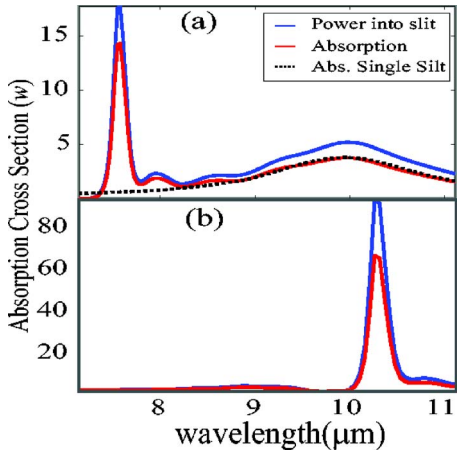

FIG. 3. (Color online) (a) Absorption cross section (red line) as a function of wavelength for $a=7.15\ \mu$m, $L=1.0\ \mu$m, $w=50$ nm, $b=0.5\ \mu$m, $d=0.425\ \mu$m, and $N_g=15$. We also show the light power transmitted into the upper aperture of the slit (blue line) normalized by the plane wave flux. The dashed line shows the absorption cross section for the single-slit device of Fig. 2(a) with w and L the same as above. (b) Absorption cross section (red line) and transmitted power into the slit (blue line) for $a=9.8\ \mu$m and $d=0.6\ \mu$m. All other parameters are as in Fig. 3(a).

at $\lambda_0=9.8\ \mu$m. In Fig. 3(a), we show a structure with a grating period $a=7.15\ \mu$m and a groove resonance at $\lambda_0=7.15\ \mu$m. We observe two peaks corresponding to the slit and grating resonances. The peak located at $\lambda\sim10.5\ \mu$m is associated with the slit since it approximately coincides with that of a single slit on a slab. The peak at $\lambda_0\sim7.15\ \mu$m, where the slit by itself does not provide a resonant mode, is due to the grating. The absorption cross section is $\sim14w$ for the grating peak and $\sim3.5w$ for the slit peak. (Notice that the absorption cross section of the slit peak is the same as the one of the single slit without the grating.) In contrast, the absorption cross section is greatly increased when the grating and groove resonances coincide with the slit resonance and they amplify each other. With the grating period at $a=9.8\ \mu$m and groove parameters chosen so that the groove resonance is at $\lambda_0=9.8\ \mu$m, we obtain an absorption cross section of $\sim64w$ [Fig. 3(b)]. In Fig. 1(b), we show the magnetic field profile at the resonance frequency for this optimized structure. The field intensity in the slit and grooves is much higher than that of the incident light indicating the presence of resonant modes. For the device fabrication, one can make a MCT ridge using lithographic means, followed by a metal deposition and lift-off process. The grating can then be defined in the metal region. The interface between metal and MCT may need to be carefully engineered.[16] The tolerance of the enhancement to slit width variations is quite good. For the device in Fig. 3(b) and for slit width variations of $w=50\pm5$ nm, the peak absorption cross section varies less than 15%.

The propagation length of surface plasmons on the gold surface at $\lambda_0=10\ \mu$m is several tens of millimeters,[17] which is much longer than the device dimensions. One might thus expect that, as more grating periods are introduced, light will be collected from a wider region, resulting in a greater enhancement. Our simulation, however, reveals that the enhancement saturates after 20 periods (or equivalently, about 200 μm in length) on both sides of the central slit are used (Fig. 4). Therefore, the propagation loss for surface plasmons on the grating surface is dominated by reradiation rather than

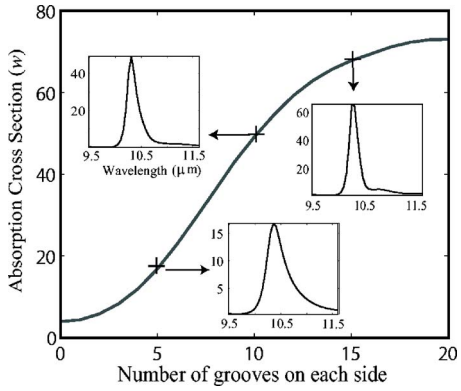

FIG. 4. Absorption cross section as a function of the number of the grooves N_g. All other parameters are as in Fig. 3(b). The insets show the spectra for $N_g=5$, 10, and 15.

material absorption. The insets in Fig. 4 show the absorption cross-section spectra for 5, 10, and 15 grooves. The peak gets higher and sharper with more grooves on the sides. With 20 grooves on either side, we can achieve an absorption cross section as large as 70w. This corresponds to an enhancement factor of ~250. The use of surface plasmons can thus strongly enhance the performance of a midinfrared photodetector. The structure considered here is polarization dependent. However, one should be able to design concentric-grating structure to provide polarization-independent enhancement.

As final remarks, the use of surface plasmons to enhance the speed of photodetectors at near-infrared wavelength range has been recently discussed in Refs. 8 and 18. Our work here represents a design of photodetector with light effectively confined into a small active detection area and hence one promising way to increase the signal/noise ratio.

The research was supported by an STTR program ran by Ray Balcerak at DARPA (Proposal No. D054-005-0094). Ravi Verma at Tanner research is gratefully acknowledged for fruitful discussions.

[1] J. Piotrowski, W. Galus, and M. Grudzi, Infrared Phys. **31**, 1 (1990).
[2] P. Norton, Opto-Electron. Rev. **10**, 159 (2002).
[3] J. J. Lee, J. D. Kim, and M. Razeghi, Appl. Phys. Lett. **73**, 602 (1998).
[4] H. J. Lezec, A. Degiron, E. Devaus, R. A. Linke, L. Martin-Moreno, F. J. Garcia-Vidal, and T. W. Ebbesen, Science **297**, 820 (2002).
[5] A. Degiron and T. W. Ebbesen, Opt. Express **12**, 3694 (2004).
[6] T. Thio, K. M. Pellerin, and R. A. Linke, Opt. Lett. **26**, 1972 (2001).
[7] F. J. Garcia-Vidal, H. J. Lezec, T. W. Ebbesen, and L. Marthin-Moreno, Phys. Rev. Lett. **90**, 213901 (2003).
[8] T. Ishi, J. Fujikata, K. Makita, T. Baba, and K. Ohashi, Jpn. J. Appl. Phys., Part 2 **44**, L364 (2005).
[9] S. D. Wu and E. N. Glytsis, J. Opt. Soc. Am. A **19**, 2018 (2002).
[10] G. Veronis, R. W. Dutton, and S. Fan, Opt. Lett. **29**, 2288 (2004).
[11] E. D. Palik, *Handbook of Optical Constants of Solids* (Academic, New York, 1985), Vol. 1, p. 286 and Vol. 2, p. 655.
[12] A. Taflove and S. C. Hagness, *Computational Electrodynamics: The Finite-Difference Time-Domain Method* (Artech House, Norwood, 2005), 3rd ed., p. 194.
[13] H. Shin, M. F. Yanik, S. Fan, R. Zia, and M. Brongersma, Appl. Phys. Lett. **84**, 4421 (2004).
[14] K. Tanaka and M. Tanaka, Appl. Phys. Lett. **82**, 1158 (2003).
[15] J. Bravo-Abad, L. Martin-Moreno, and F. J. Garcia-Vidal, Phys. Rev. E **69**, 026601 (2004).
[16] D. L. Smith, D. K. Aach, R. A. Wood, and M. W. Scott, Appl. Phys. Lett. **45**, 83 (1984).
[17] E. N. Economou, Phys. Rev. **182**, 539 (1969).
[18] L. Tang, D. A. B. Miller, A. K. Okyay, J. A. Matteo, Y. Yuen, K. C. Saraswat, and L. Hesselink, Opt. Lett. **31**, 1519 (2006).